SIAM J. SCI. COMPUT.
Vol. 35, No. 3, pp. A1440–A1460

APPROXIMATION OF QUANTITIES OF INTEREST IN STOCHASTIC PDEs BY THE RANDOM DISCRETE L^2 PROJECTION ON POLYNOMIAL SPACES*

G. MIGLIORATI†, F. NOBILE‡, E. VON SCHWERIN§, AND R. TEMPONE¶

Abstract. In this work we consider the random discrete L^2 projection on polynomial spaces (hereafter RDP) for the approximation of scalar quantities of interest (QOIs) related to the solution of a partial differential equation model with random input parameters. In the RDP technique the QOI is first computed for independent samples of the random input parameters, as in a standard Monte Carlo approach, and then the QOI is approximated by a multivariate polynomial function of the input parameters using a discrete least squares approach. We consider several examples including the Darcy equations with random permeability, the linear elasticity equations with random elastic coefficient, and the Navier–Stokes equations in random geometries and with random fluid viscosity. We show that the RDP technique is well suited to QOIs that depend smoothly on a moderate number of random parameters. Our numerical tests confirm the theoretical findings in [G. Migliorati, F. Nobile, E. von Schwerin, and R. Tempone, *Analysis of the Discrete L^2 Projection on Polynomial Spaces with Random Evaluations*, MOX report 46-2011, Politecnico di Milano, Milano, Italy, submitted], which have shown that, in the case of a single uniformly distributed random parameter, the RDP technique is stable and optimally convergent if the number of sampling points is proportional to the square of the dimension of the polynomial space. Here optimality means that the weighted L^2 norm of the RDP error is bounded from above by the best L^∞ error achievable in the given polynomial space, up to logarithmic factors. In the case of several random input parameters, the numerical evidence indicates that the condition on quadratic growth of the number of sampling points could be relaxed to a linear growth and still achieve stable and optimal convergence. This makes the RDP technique very promising for moderately high dimensional uncertainty quantification.

Key words. PDE stochastic data, discrete least squares, polynomial approximation

AMS subject classifications. 41A10, 65N35

DOI. 10.1137/120897109

1. Introduction.

In recent years, the modeling of uncertainty in mathematical models has attracted a lot of attention in the scientific community. When a probabilistic framework is considered, uncertainty in the model parameters is modeled

*Submitted to the journal's Methods and Algorithms for Scientific Computing section October 30, 2012; accepted for publication (in revised form) March 1, 2013; published electronically May 30, 2013. The work of the first and second authors was supported by the Italian grant FIRB-IDEAS (Project RBID08223Z) "Advanced numerical techniques for uncertainty quantification in engineering and life science problems." They also received support from the Center for ADvanced MOdeling Science (CADMOS).

http://www.siam.org/journals/sisc/35-3/89710.html

†Corresponding author. MATHICSE-CSQI, École Polytechnique Fédérale de Lausanne, Lausanne CH-1015, Switzerland, and MOX-Dipartimento di Matematica "Francesco Brioschi," Politecnico di Milano, Milano 20133, Italy (giovanni.migliorati@gmail.com).

‡MATHICSE-CSQI, École Polytechnique Fédérale de Lausanne, Lausanne CH-1015, Switzerland, and MOX-Dipartimento di Matematica "Francesco Brioschi," Politecnico di Milano, Milano 20133, Italy (fabio.nobile@epfl.ch).

§MATHICSE-CSQI, École Polytechnique Fédérale de Lausanne, Lausanne CH-1015, Switzerland, and Applied Mathematics and Computational Sciences, KAUST, Thuwal 23955-6900, Saudi Arabia (erik.vonschwerin@epfl.ch).

¶Applied Mathematics and Computational Sciences, and SRI Center for Uncertainty Quantification in Computational Science and Engineering, KAUST, Thuwal 23955-6900, Saudi Arabia (raul.tempone@kaust.edu.sa). This author's work was partially supported by the Academic Excellency Alliance UT Austin–KAUST project "Predictability and uncertainty quantification for models of porous media."

in terms of random variables. The underlying challenge concerns the accurate and efficient approximation of the model outcome in the presence of many random input parameters. In the context of partial differential equations (PDEs) with stochastic data, a well-established technique that has been used in many engineering applications [7, 13, 10] consists in the use of a spectral expansion to represent the input/output dependence; see, e.g., [11, 18, 14]. Once such an expansion has been computed by some means, statistics of the model output can easily be recovered. The *random discrete L^2 projection* (RDP), also known as regression or point collocation approach, has been proposed in the context of applications devoted to uncertainty analysis in [13, 3, 8] as a tool for computing the spectral expansion of the model response. The regression approach is based on the evaluation of the target output function on randomly selected points and aims to improve the slow convergence of the classical Monte Carlo method by performing a discrete projection onto a multivariate polynomial space. It differs from other techniques based on a deterministic choice of the points at which the function is evaluated, also known as *collocation methods on sparse grids* [4].

In [16, 5, 15] the RDP was analyzed in the context of approximating a smooth aleatory function in the L^2 probability sense. This approximation problem falls in the field of nonparametric regression with random design, and when noise is present there exist well-known estimates for the approximation error [12]. The RDP of a given aleatory function consists in its discrete L^2 projection over a polynomial space, and is computed by evaluating the target function pointwise in randomly selected points of the parameter space. Unlike the usual nonparametric regression in statistics, the evaluations are assumed to be noise-free. The stability and convergence properties of RDP are analyzed in [16, 5]. Under some assumptions on the probability density, it is proved in these works that, in one dimension and when the number of sampling points is proportional to the square of the dimension of the polynomial space, the RDP converges optimally in the sense that the L^2 error behaves like the best approximation error (measured in the "sup" norm) of the target function in the chosen polynomial space, up to logarithmic factors. It is reasonable to compare with the L^∞ best approximation error since the RDP is based on pointwise evaluations. In [5] a bound in terms of the best approximation in the L^2 norm is obtained by taking expectations. In contrast the bound in [16] is in terms of the L^∞ norm and holds with high probability. The above-mentioned quadratic relation between the number of sampling points and the dimension of the polynomial space actually guarantees the stability of the RDP. Several numerical tests in [16] show the capabilities of the method and highlight the influence of the dimension of the parameter space and of the smoothness of the target function on the achieved convergence rate. Further theoretical results and numerical applications can be found in [15].

The present work focuses on the application of RDP to the approximation of QOIs related to the solution of PDEs with stochastic data. The aleatory function is defined as a functional of the solution of the PDE, e.g., an integral over a portion of the physical domain. We begin by considering the Darcy model with a random diffusion coefficient, parametrized in a one-dimensional parameter space. The randomness affects the value of the coefficient in a particular region of the physical domain, for instance, an inclusion. Then we investigate a variation of the Darcy example where the randomness affects the location where the diffusion coefficient is discontinuous. Thus the example treats an inclusion with a random domain in the sense that the geometrical shape of the domain is parametrized in terms of a random variable.

Next, we move to higher dimensional parameter spaces, always using the isotropic

total degree polynomial space (defined in section 2). This choice is well motivated in cases where the target function depends analytically on each input parameter with the analyticity region not affected by the other parameters [2]. We consider a Darcy model with a random diffusion coefficient parametrized in a five-dimensional parameter space, increasing to five the number of nonoverlapping inclusions that are displaced in the physical domain.

Finally, we consider two more complex vectorial problems: the Navier–Lamé equations that govern the bending of a cantilever beam in the regime of linear elasticity, and the incompressible Navier–Stokes equations that govern the motion of a viscous fluid in a pipe. Both examples contain uncertainty in the model parameters: the Young modulus in the former, and the viscosity and the geometry of the domain in the latter.

All examples of the elliptic class presented in this paper, with one-dimensional parameter space, validate the theoretical results outlined in [16, 5]. In particular, having a number of sampling points proportional to the square of the dimension of the polynomial space always yields optimal convergence, as predicted by the theory. Moreover, when approximating a smooth function an optimal convergence is observed up to a certain threshold even if the number of sampling points is only linearly proportional to the dimension of the polynomial space. Beyond such a threshold, the error starts diverging. On the other hand, in all examples with higher dimensional parameter space, the optimal convergence rate for smooth functions has always been achieved, even with a linear proportionality between the number of sampling points and the dimension of the polynomial space. No blow-up has been observed in all ranges of polynomial space dimensions tested. This is consistent with the observation in [16]: when the dimension gets higher, the RDP seems to become stable even when the number of sample points is only linearly proportional to the dimension of the polynomial space. In this sense, the one-dimensional case is the most ill-conditioned case, making the RDP more promising in moderately high dimensional approximation problems.

The outline of the paper is the following: in section 2 we introduce the formulation of the random discrete L^2 projection and recall the main results obtained in [16] concerning stability and optimality. In section 3 the numerical examples are presented. Examples 1, 2, and 3 are based on the Darcy model with random permeability. Examples 4 and 5 address the linear elasticity equations with random elastic coefficient and Navier–Stokes equations in random geometries and with random fluid viscosity. Finally, section 4 contains the concluding discussion.

2. The random discrete L^2 projection on polynomial spaces. In this section we review the formulation of the random discrete L^2 projection in an abstract setting and recall the main results obtained in [16]. The technique will then be applied to PDEs with random data in section 3.

Let $\Gamma \subseteq \mathbb{R}^N$ be an N-dimensional subset of the N-dimensional Euclidean space, with a tensor structure form $\Gamma = \Gamma^1 \times \cdots \times \Gamma^N$. Denote by $\rho : \Gamma \to \mathbb{R}^+$ a probability density function over Γ, and by $\mathbf{Y} = (Y_1, \ldots, Y_N)$ a vector of N random variables, taking values in Γ and distributed according to the density ρ.

We consider a random variable $Z = \phi(\mathbf{Y})$, where $\phi : \Gamma \to \mathbb{R}$ is assumed to be a smooth function, and we are interested in computing statistical moments of Z. This will be achieved by first constructing a reduced model; i.e., we approximate the function $\phi(Y_1, \ldots, Y_N)$ by a suitable multivariate polynomial $\phi_\Lambda(Y_1, \ldots, Y_N)$. We then compute statistical moments using the approximate function ϕ_Λ.

We denote by

$$\mathbb{E}[Z] := \int_\Gamma \phi(\mathbf{y})\rho(\mathbf{y})d\mathbf{y}$$

the expected value of the random variable $Z = \phi(\mathbf{Y})$, and by

$$Pr(A) := \int_A \rho(\mathbf{y})d\mathbf{y}$$

the probability of the event $A \in \mathcal{B}(\Gamma)$, where $\mathcal{B}(\Gamma)$ is the Borel σ-algebra with respect to the measure $\rho(\mathbf{y})d\mathbf{y}$. Throughout the paper we also assume the following.

Assumption 1. Γ is a bounded set, and $0 < \rho_{\min} \leq \rho(\mathbf{y}) \leq \rho_{\max} < \infty$ for all $\mathbf{y} \in \Gamma$.

Remark 1. This assumption excludes, e.g., the normal and lognormal cases, since these densities are not bounded away from zero due to their unbounded support. In the case of densities with unbounded support, e.g., normal and lognormal, derivations of results corresponding to Propositions 2.1 and 2.4 and Theorem 2.2 would have to rely on the use of suitable weighted L^∞ norms (see, e.g., [1]), but this is beyond the scope of the present paper.

We introduce the space L^2_ρ of square integrable functions $f : \Gamma \to \mathbb{R}$, endowed with the norm

$$\|f\|_{L^2_\rho} = \left(\int_\Gamma f^2(\mathbf{y})\rho(\mathbf{y})d\mathbf{y} \right)^{1/2}.$$

Let $\mathbf{p} = (p_1, \ldots, p_N)$ be a multi-index and $\Lambda \subset \mathbb{N}^N$ a set of multi-indices. In what follows we consider only sets Λ that are monotone in the following sense.

PROPERTY 1 (monotonicity of Λ). *Consider two multi-indices $\mathbf{p}', \mathbf{p}'' \in \mathbb{N}^N$ such that $p''_n \leq p'_n$ for all $n = 1, \ldots, N$. The multi-index set Λ is monotone if the following holds:*

$$\mathbf{p}' \in \Lambda \Longrightarrow \mathbf{p}'' \in \Lambda.$$

We denote by $\mathbb{P}_\Lambda(\Gamma)$ the multivariate polynomial space

$$\mathbb{P}_\Lambda(\Gamma) = \text{span}\left\{ \prod_{n=1}^N y_n^{p_n}, \text{ with } \mathbf{p} \in \Lambda \right\}, \tag{2.1}$$

and by $\#\Lambda = \dim(\mathbb{P}_\Lambda)$ the dimension of the polynomial space, which corresponds to the cardinality of the multi-index set Λ. For convenience, the set Λ can be arranged in lexicographical order, and according to this order, we can denote by $\mathbf{p}^j$ the jth multi-index of Λ. Sometimes we refer to the elements of Λ with the generic multi-index $\mathbf{p}$, rather than listing them by the lexicographical index.

Since the monomial basis in (2.1) is very ill-conditioned, in practice we use an orthonormal polynomial basis. A typical choice is to take orthogonal polynomials with respect to the measure $\rho(\mathbf{y})d\mathbf{y}$. We introduce an N-dimensional orthonormal polynomial basis $\{l_j\}_{j=1}^{\#\Lambda}$ of $\mathbb{P}_\Lambda$ with respect to the weighted inner product

$$(u, v)_{L^2_\rho} = \int_\Gamma u(\mathbf{y})v(\mathbf{y})\rho(\mathbf{y})\, d\mathbf{y},$$

i.e., $(l_i, l_j)_{L^2_\rho} = \delta_{ij}$. Assumption 1 ensures that the orthonormal basis is complete in L^2_ρ when $\Lambda = \mathbb{N}^N$, applying Theorems 3.3 and 3.5 of [9].

In the particular case where the density factorizes as $\rho(\mathbf{y}) = \prod_{n=1}^N \rho_n(y_n)$, the basis can be constructed by tensorizing one-dimensional orthogonal polynomials with respect to each weight ρ_n separately. Given n, let $\{\varphi_j^n(\cdot)\}_j$ be the orthogonal polynomials with respect to ρ_n. The jth multi-index $\mathbf{p}^j \in \Lambda$ is associated with the corresponding jth multidimensional basis function by

$$l_j(\mathbf{y}) = \prod_{n=1}^N \varphi^n_{p_n^j}(y_n). \tag{2.2}$$

Thus, using the basis functions provided by (2.2), the definition (2.1) of $\mathbb{P}_\Lambda$ becomes

$$\mathbb{P}_\Lambda(\Gamma) = \operatorname{span}\{l_j,\, j = 1, \dots, \#\Lambda\}, \tag{2.3}$$

and of course $\dim(\mathbb{P}_\Lambda) = \#\Lambda$. Observe that in general (2.1) and (2.3) are equivalent only if the index set Λ satisfies the monotonicity property, Property 1.

We consider a sample $\mathbf{y}_1, \dots, \mathbf{y}_M$ of size $M \geq \#\Lambda$ of independent random variables identically distributed according to the density ρ, and then evaluate the function ϕ pointwise at each value $\mathbf{y}_i$, $i = 1, \dots, M$.

Finally, we compute a discrete least squares approximation of the values $\phi(\mathbf{y}_i)$ in the polynomial space $\mathbb{P}_\Lambda$, i.e.,

$$\phi_\Lambda = \Pi_M^{\Lambda,\omega}\phi = \operatorname*{argmin}_{v \in \mathbb{P}_\Lambda(\Gamma)} \frac{1}{M} \sum_{i=1}^M (\phi(\mathbf{y}_i) - v(\mathbf{y}_i))^2. \tag{2.4}$$

We will use the superscript (or subscript) ω to denote a quantity that depends on the random sample $\mathbf{y}_1, \dots, \mathbf{y}_M$ (and therefore is random itself).

We now introduce the *random* discrete inner product

$$(u, v)_{M,\omega} = \frac{1}{M} \sum_{i=1}^M u(\mathbf{y}_i) v(\mathbf{y}_i) \tag{2.5}$$

on $\mathbb{P}_\Lambda(\Gamma)$, and the corresponding discrete norm $\|u\|_{M,\omega} = (u, u)^{1/2}_{M,\omega}$. Note that for $M \geq \#\Lambda$ the bilinear form (2.5) is an inner product on $\mathbb{P}_\Lambda(\Gamma)$ with probability one, by Assumption 1. With this notation we can write (2.4) as

$$\text{find } \Pi_M^{\Lambda,\omega}\phi \in \mathbb{P}_\Lambda(\Gamma) \quad \text{such that} \quad (\phi - \Pi_M^{\Lambda,\omega}\phi, v)_{M,\omega} = 0 \quad \forall\, v \in \mathbb{P}_\Lambda(\Gamma).$$

Some of the most common choices of function spaces are tensor product, total degree, and hyperbolic cross, which are defined by the index sets below. We index the set Λ by the subscript w, which denotes the maximum polynomial degree used:

$$\text{tensor product (TP)}, \quad \Lambda_{\mathrm{w}} = \Big\{\mathbf{p} \in \mathbb{N}^N : \max_{n=1,\dots,N} p_n \leq \mathrm{w}\Big\}, \tag{2.6}$$

$$\text{total degree (TD)}, \quad \Lambda_{\mathrm{w}} = \Big\{\mathbf{p} \in \mathbb{N}^N : \sum_{n=1}^N p_n \leq \mathrm{w}\Big\}, \tag{2.7}$$

$$\text{hyperbolic cross (HC)}, \quad \Lambda_{\mathrm{w}} = \Big\{\mathbf{p} \in \mathbb{N}^N : \prod_{n=1}^N (p_n + 1) \leq \mathrm{w} + 1\Big\}. \tag{2.8}$$

These spaces are isotropic in the sense that the maximum polynomial degree w is the same in all variables $Y_1, \dots, Y_N$. The dimensions of the TP and TD spaces are

$$\#TP(\mathrm{w}, N) = (\mathrm{w}+1)^N, \tag{2.9}$$

$$\#TD(\mathrm{w}, N) = \binom{N+\mathrm{w}}{N}. \tag{2.10}$$

The dimension of the HC space is harder to quantify. An upper bound is given by

$$\#HC(\mathrm{w}, N) \leq \lfloor (\mathrm{w}+1) \cdot (1+\log(\mathrm{w}+1))^{N-1} \rfloor, \tag{2.11}$$

where $\lfloor \cdot \rfloor$ denotes the operation of rounding a real number downwards to the nearest integer. This bound is sharp for $N = 2$ and becomes very conservative as N increases.

2.1. Stability and convergence rate of the random discrete L^2 projection. Here we recall some theoretical results concerning the discrete L^2 projection, derived in [16] and [5]. Let us first introduce the quantity

$$C^\omega(M, \Lambda) := \sup_{v \in \mathbb{P}_\Lambda \setminus \{v \equiv 0\}} \frac{\|v\|^2_{L^2_\rho}}{\|v\|^2_{M,\omega}}, \tag{2.12}$$

which depends on the random sample and is therefore a random variable. The following proposition states the optimality of the discrete L^2 projection with respect to the L^∞ norm, when the error is evaluated in the L^2_ρ norm.

PROPOSITION 2.1 (see [16]). *With $C^\omega(M, \Lambda)$ defined as in* (2.12)*, it holds that*

$$\|\phi - \Pi^{M,\omega}_\Lambda \phi\|_{L^2_\rho} \leq \left(1 + \sqrt{C^\omega(M, \Lambda)}\right) \inf_{v \in \mathbb{P}_\Lambda(\Gamma)} \|\phi - v\|_{L^\infty}. \tag{2.13}$$

As a consequence, the convergence properties of the RDP are strictly related to the properties of the quantity $C^\omega(M, \Lambda)$. The next theorem quantifies the asymptotic behavior of the random variable $C^\omega(M, \Lambda)$.

THEOREM 2.2 (see [16]). *Let $C^\omega(M, \Lambda)$ be the random variable defined in* (2.12)*. Then, for any given Λ we have*

$$\lim_{M \to \infty} C^\omega(M, \Lambda) = 1 \quad \textit{a.s.}$$

The previous proposition and theorem are general results on the discrete L^2 projection: they hold in any dimension N, for any arbitrary N-dimensional monotone multi-index set Λ, and for any density ρ satisfying Assumption 1.

When $N = 1$ and $\rho = \mathcal{U}([-1, 1])$, a probability estimate has been proved in [16]. In this particular case the polynomial space is denoted by $\mathbb{P}_\mathrm{w}$ rather than $\mathbb{P}_\Lambda$, because the multi-index set Λ is just $\{0, 1, \dots, \mathrm{w}\}$ and its dimension $\#\Lambda = 1 + \mathrm{w}$. Accordingly, the projector $\Pi^{M,\omega}_\Lambda$ is denoted by $\Pi^{M,\omega}_\mathrm{w}$. The following theorem ensures the stability and accuracy of the discrete L^2 projection, under the condition $M \propto (\#\Lambda)^2$.

THEOREM 2.3 (see [16]). *For any $\delta \in (0, 1)$, under the condition*

$$\frac{M}{3 \log((M+1)/\delta)} \geq 4\sqrt{3}\,\mathrm{w}^2 \tag{2.14}$$

it holds

$$Pr\left(\|\phi - I\!I_{\mathrm{w}}^{M,\omega}\phi\|_{L^2_\rho} \le \left(1+\sqrt{3\log\frac{M+1}{\delta}}\right)\inf_{v\in\mathbb{P}_{\mathrm{w}}}\|\phi - v\|_{L^\infty}\right) \ge 1-\delta. \tag{2.15}$$

We remark that in practice condition (2.14) is equivalent to $M \propto (\#\Lambda)^2$, since the effect due to the presence of the nonoptimal logarithmic factor is often negligible. In [5] an estimate in expectation of the error $\|\phi - I\!I_{\mathrm{w}}^{M,\omega}\phi\|_{L^2_\rho}$ has also been derived, showing that it behaves as the L^2 best approximation error under the same condition $M \propto (\#\Lambda)^2$. Moreover, for analytic functions, the best approximation error converges exponentially as w increases. Notice that, to keep condition (2.14) satisfied, increasing w requires increasing M as well.

There also exists a general relation between the optimal convergence rate of the random projection and its stability, which holds again in any dimension N and for any Λ and ρ. The same random variable C^ω, besides entering into the error estimate (2.13), plays a role in the stability of the random projection, as stated in the next proposition. As in [16], we denote by D^ω the random design matrix associated with problem (2.4); its elements are defined as $[D^\omega]_{i,j} = l_j(\mathbf{y}_i)$.

PROPOSITION 2.4 (from [16]). *The spectral condition number (2 norm) of the matrix $(D^\omega)^T D^\omega$ is equal to*

$$cond\Big((D^\omega)^T D^\omega\Big) = c^\omega(M,\Lambda)\, C^\omega(M,\Lambda), \tag{2.16}$$

where

$$c^\omega(M,\Lambda) := \sup_{v\in\mathbb{P}_\Lambda\setminus\{v\equiv 0\}} \frac{\|v\|^2_{M,\omega}}{\|v\|^2_{L^2_\rho}}. \tag{2.17}$$

Remark 2. It is also possible to construct an RDP approximation $\widetilde{I\!I}_{\mathrm{w}}^{M,\omega}\phi$ in which the sampling points are drawn from a density $\widetilde{\rho}$ different from ρ. Assuming that $\rho(\mathbf{y})/\widetilde{\rho}(\mathbf{y}) < +\infty$ for all $\mathbf{y}\in\Gamma$, the following error bound will hold:

$$\|\phi - \widetilde{I\!I}_{\mathrm{w}}^{M,\omega}\phi\|_{L^2_\rho(\Gamma)} \le \left\|\frac{\rho}{\widetilde{\rho}}\right\|^{\frac{1}{2}}_{L^\infty(\Gamma)} \|\phi - \widetilde{I\!I}_{\mathrm{w}}^{M,\omega}\phi\|_{L^2_{\widetilde{\rho}}(\Gamma)}. \tag{2.18}$$

We then propose choosing the density $\widetilde{\rho}$ so as to improve the stability of RDP while preserving its accuracy. A good candidate is given by the Chebyshev distribution. Indeed, it has been shown in [5] that when drawing samples from the monovariate Chebyshev distribution, the RDP is stable and optimally convergent under the assumption $M \propto \#\Lambda$, which is much less demanding than (2.14).

3. Parametric PDEs. In [16] we presented some numerical examples of RDP to approximate monovariate and multivariate target functions $\phi = \phi(\mathbf{y}) : \Gamma \to \mathbb{R}$ on polynomial spaces. The role of smoothness was investigated. When using a relation $M \propto (\#\Lambda)^2$, an optimal (in the sense described in the introduction) convergence rate was always observed. On the other hand, when using a linear relation $M \propto \#\Lambda$, the optimal convergence rate was observed up to a certain threshold, after which the error started increasing and eventually diverged. This effect was clearly observed in the monovariate case. However, in higher dimensions the blow-up of the error was not observed in the range of practical polynomial degrees explored. As pointed out

in [16], the linear relation $M \propto \#\Lambda$ therefore seems to be sufficient for all practical purposes to achieve an accurate and stable approximation.

The aim of this paper is to test the RDP when the target function ϕ is related to the solution of a stochastic PDE model. We focus on QOIs of integral type over the spatial domain of the PDE model, such as the mean of the solution or its gradient in portions of the domain, or pointwise quantities such as the maximum or minimum of the solution in the domain.

Consider a steady state PDE model,

$$\mathcal{L}(\mathbf{x}, \mathbf{y}, u, f, g, \Omega) = 0, \tag{3.1}$$

defined on a bounded domain $\Omega \subset \mathbb{R}^d$ and parametrized by $\mathbf{y} \in \Gamma \subseteq \mathbb{R}^N$, with $u : \Omega \times \Gamma \to \mathbb{R}$ its solution, $f : \Omega \times \Gamma \to \mathbb{R}$ the forcing term, and $g : \partial\Omega \times \Gamma \to \mathbb{R}$ a suitable boundary condition. In general, the operator $\mathcal{L}$ can be nonlinear with respect to the solution u of the model. The following examples feature only two-dimensional spatial domains Ω; i.e., $d = 2$. However, extensions to three-dimensional problems are straightforward. The domain may also depend on the parameter $\mathbf{y}$; i.e., $\Omega = \Omega(\mathbf{y})$. Moreover, we assume that f and g satisfy proper conditions to make the whole model well-posed in the sense of Hadamard.

Considering $\mathbf{y} \in \Gamma$ as a realization of the random variable $\mathbf{Y}$ distributed according to the density $\rho : \Gamma \to \mathbb{R}^+$, the parametric model (3.1) can also be considered as a PDE model with stochastic data.

We now proceed with some examples to illustrate the application of the RDP to approximate QOIs depending on the solution of stochastic PDEs. First we focus on models in the elliptic class, where the solution typically depends smoothly on the random variable, as proved in [6, 1].

The first three examples concern the Darcy flow in a medium containing some inclusions. The first and second examples have a one-dimensional stochastic parameter space: in Example 1 the value of the diffusion coefficient is stochastic, while in Example 2 the geometrical shape of the inclusion is stochastic. In Example 3 we increase the dimension of the parameter space to five.

Then we analyze the linear elasticity model and the incompressible Navier–Stokes model. The former exhibits a highly regular dependence of the solution on the random parameter affecting *Young's modulus*, while the latter shows some nonsmooth QOIs.

To quantify the error $\|\phi - \mathit{\Pi}_\Lambda^{M,\omega}\phi\|_{L^2_\rho}$ committed by RDP we employ the cross-validation procedure described in [16, section 4]. A random set of 100 cross-validating points is chosen at the beginning. Then the cross-validated error in the ∞ norm is defined as

$$\|\phi - \mathit{\Pi}_\Lambda^{M,\omega}\phi\|_{cv} = \max_{\mathbf{z}_j} |\phi(\mathbf{z}_j) - \mathit{\Pi}_\Lambda^{M,\omega}\phi(\mathbf{z}_j)|, \tag{3.2}$$

where $\mathbf{z}_j$, $j = 1, \ldots, 100$, is the set of cross-validation points. To estimate the variability of (3.2) due to the random sampling of the M collocation points, we have repeated the calculation over R independent sets of points $\mathbf{y}_j^{\omega_k}, j = 1, \ldots, M$, with $k = 1, \ldots, R$, and we have computed the average error

$$\overline{E}_{cv} = \frac{\sum_{k=1}^{R} \|\phi - \mathit{\Pi}_\Lambda^{M,\omega}\phi\|_{cv}}{R}, \tag{3.3}$$

as well as the sample standard deviation by

$$s_E = \sqrt{\frac{1}{R-1}\sum_{k=1}^{R}\left(\|\phi - I\!\Pi_{\Lambda}^{M,\omega}\phi\|_{cv} - \overline{E}_{cv}\right)^2}. \tag{3.4}$$

We also aim to analyze the condition number of $(D^\omega)^T D^\omega$ that has been introduced in (2.16). Following [16, section 4], it can be quantified as

$$\mathrm{cond}\Big((D^\omega)^T D^\omega\Big) = \frac{\sigma_{\max}\Big((D^\omega)^T D^\omega\Big)}{\sigma_{\min}\Big((D^\omega)^T D^\omega\Big)}, \tag{3.5}$$

where $\sigma_{\max}(\cdot)$ and $\sigma_{\min}(\cdot)$ are the maximum and minimum singular values. Again, denoting by D^{ω_k} the design matrix built with the kth set $\{\mathbf{y}_j^{\omega_k}\}_j$, we estimate the mean condition number $\overline{K}$ over the R repetitions as

$$\overline{K} = \frac{\sum_{k=1}^{R}\mathrm{cond}\Big((D^{\omega_k})^T D^{\omega_k}\Big)}{R}, \tag{3.6}$$

and the standard deviation as

$$s_K = \sqrt{\frac{1}{R-1}\sum_{k=1}^{R}\left(\mathrm{cond}\Big((D^{\omega_k})^T D^{\omega_k}\Big) - \overline{K}\right)^2}. \tag{3.7}$$

In the convergence plots in Figures 3.2–3.6, 3.8, 3.9, 3.11, and 3.13, the continuous lines mark the mean of the error $\|\phi - I\!\Pi_{\Lambda}^{M,\omega}\phi\|_{L^2_\rho}$, or the mean of the condition number of the random design matrix, while the dashed lines mark the mean plus one standard deviation. The discretization of the PDE model over the spatial domain Ω is obtained by means of the finite element method. In Examples 1–4 the P1 finite elements are used. In Example 5 the inf-sup compatible P2-P1 finite elements are used.

3.1. Example 1: The Darcy flow in a domain with one inclusion. To start, we consider an elliptic model on a bounded deterministic domain $\Omega \subset \mathbb{R}^2$, with a random diffusion coefficient μ:

$$\begin{cases} -\nabla\cdot(\mu(\mathbf{x},\mathbf{y})\,\nabla u(\mathbf{x},\mathbf{y})) = 0, & \mathbf{x} \text{ in } \Omega,\ \mathbf{y}\in\Gamma,\\ u(\mathbf{x},\mathbf{y}) = g_1(\mathbf{x}), & \mathbf{x} \text{ on } \partial\Gamma_1\cup\partial\Gamma_3,\ \mathbf{y}\in\Gamma,\\ \partial_\nu u(\mathbf{x},\mathbf{y}) = g_2(\mathbf{x}), & \mathbf{x} \text{ on } \partial\Gamma_2\cup\partial\Gamma_4,\ \mathbf{y}\in\Gamma. \end{cases} \tag{3.8}$$

We set problem (3.8) in a unitary square domain, with a circular inclusion Ω_I with radius 0.2, as shown in Figure 3.1. The edges are labeled clockwise as $\Gamma_1, \Gamma_2, \Gamma_3, \Gamma_4$ starting from the left. We impose nonhomogeneous Dirichlet conditions on the vertical edges and homogeneous Neumann conditions on the horizontal ones, to force a steady state flow from left to right. The random diffusion coefficient depends on a uniform random variable $Y \sim \mathcal{U}(-1,1)$ and is defined as

$$\mu(\mathbf{x}, Y) = \begin{cases} \exp(5\,Y), & \Omega_I,\\ 10^{-4}, & \Omega\setminus\Omega_I. \end{cases} \tag{3.9}$$

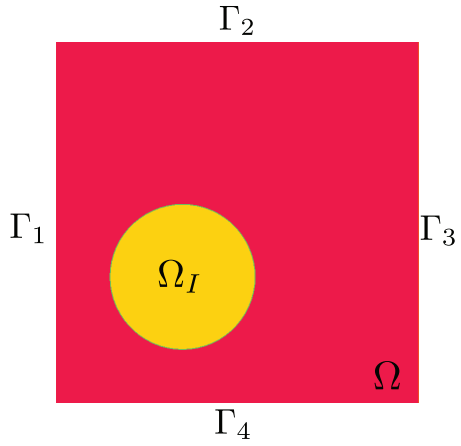

FIG. 3.1. *Square domain Ω with a circular inclusion Ω_I.*

Such a model for the coefficient can be employed in practical situations where the value of the diffusion properties of the material are not accurately determined in a given region of the physical domain, or when the value is a function of the outcome of some stochastic process with a known underlying probability law. Notice that the aforementioned diffusion coefficient may jump by more than four orders of magnitude from the bulk to the inclusion.

The QOIs we analyze are defined by integrals of the solution over the physical domain. We consider the mean of the solution u in Ω,

$$\mathrm{QOI}_1(u) = \frac{1}{|\Omega|}\int_\Omega u\, d\Omega; \tag{3.10}$$

the mean of $|\nabla u|^2$ in Ω,

$$\mathrm{QOI}_2(u) = \frac{1}{|\Omega|}\int_\Omega |\nabla u|^2\, d\Omega; \tag{3.11}$$

and the mean of the solution on the left boundary segment Γ_1,

$$\mathrm{QOI}_3(u) = \frac{1}{|\Gamma_1|}\int_{\Gamma 1} u\, d\Omega. \tag{3.12}$$

All these QOIs are analytic functions of the parameter $\mathbf{y}$ (see, e.g., [1, 6]) so we expect the best approximation error to decay exponentially fast with respect to the polynomial degree w. The numerical results obtained with a sample size chosen as $M \propto \#\Lambda$ are reported in Figure 3.2, where we plot the condition number (3.5) of the matrix $(D^\omega)^T D^\omega$ (top-left) and the error in the QOI (measured using (3.2)) versus the polynomial degree.

When the value of the proportionality constant c decreases too much, the convergence rate achieved by the random projection is reduced, and the variability of the error amplifies as well. Analogous results were shown in [16] for scalar target functions.

Figure 3.3 shows the results for QOI_1 in the case of a sample size $M \propto (\#\Lambda)^2$. We see that, as the proportionality constant increases, the convergence curve "stabilizes"

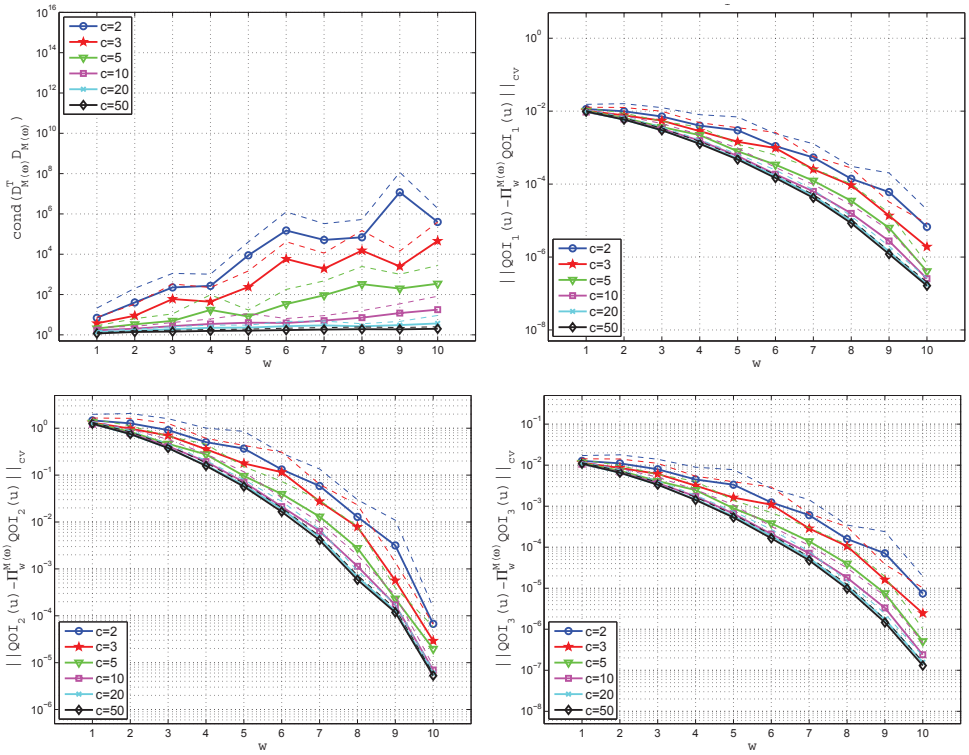

FIG. 3.2. *Example* 1. *Condition number* (3.5) *(top-left) and approximation errors* (3.2) *in the* QOI_i, $i = 1, 2, 3$, *using* $M = c \cdot \#\Lambda = c \cdot (\mathrm{w} + 1)$. *Continuous lines: sample mean averaged over* $R = 100$ *repetitions. Dashed lines: sample mean plus one sample standard deviation averaged over* $R = 100$ *repetitions.*

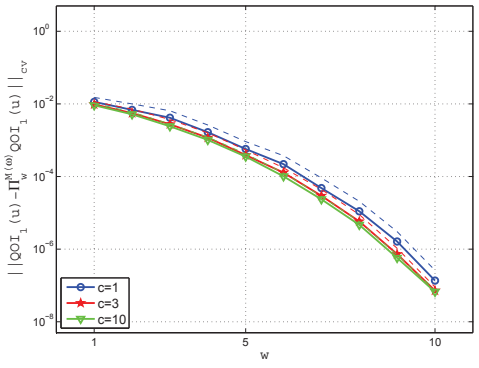

FIG. 3.3. *Example* 1. *Approximation errors* (3.2), *using* $M = c \cdot (\#\Lambda)^2 = c \cdot (\mathrm{w}+1)^2$. *Continuous lines: sample mean averaged over* $R = 100$ *repetitions. Dashed lines: sample mean plus one sample standard deviation averaged over* $R = 100$ *repetitions.*

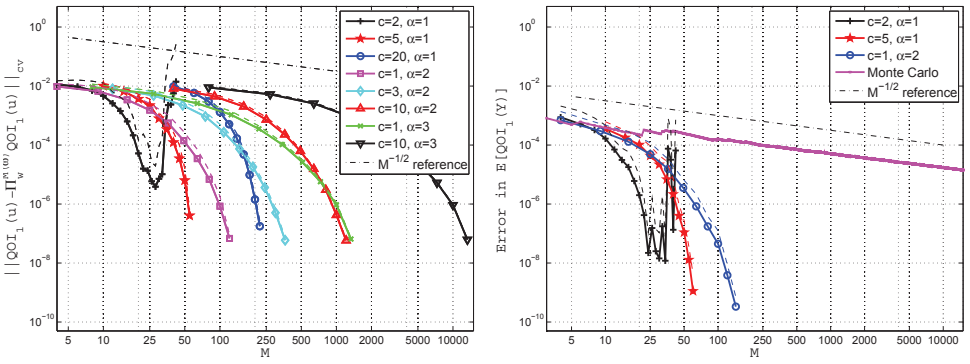

FIG. 3.4. *Example* 1. *Left: approximation errors* (3.2) *in the* QOI_1 *versus* M *for different choices of the sample size,* $M = c \cdot (\#\Lambda)^\alpha = c \cdot (\mathrm{w}+1)^\alpha$. *The markers are used to indicate progressive values of* w, *starting from* $\mathrm{w} = 1$. *Right: errors in the scalar quantity* $\mathbb{E}[QOI_1]$ *versus* M. *Here* $\mathbb{E}[QOI_1]$ *was approximated from the RDP reduced model, and the error was evaluated using a highly accurate reference solution computed with* $\mathrm{w} = 20$ *and* $M = 5 \cdot (\mathrm{w}+1)^2$*; the continuous curves show the mean error over* $R = 100$ *repetitions, and the dashed lines show the mean error plus one sample standard deviation. The estimated standard deviation of the sample mean in a simple Monte Carlo approximation of* $\mathbb{E}[QOI_1]$ *is also included.*

onto a limit curve that corresponds to the optimal convergence, i.e., the convergence of the exact L^2 projection. Note that Figures 3.2 and 3.3 give convergence plots in terms of the dimension of the polynomial space. However, the actual cost of RDP is proportional to the sample size M; therefore it is also useful to look at convergence plots of error versus M. Note that Figure 3.2 (top-right) and Figure 3.3 were based on the same data sets, but including only values of $\mathrm{w} \leq 10$. This is shown in Figure 3.4, where error plots for QOI_1 are shown for different choices of proportionality relation $M \propto (\#\Lambda)^\alpha$.

Observe that the choice $M \propto (\#\Lambda)^2$, which according to the theoretical estimates is the minimal relation that guarantees stability of the projection, leads to exponential convergence. Choosing a smaller sample size, e.g., $M = 2 \cdot \#\Lambda$, yields a faster convergence with respect to M up to a certain threshold, after which the solution deteriorates. This effect is also seen in [16, Figure 8].

As an example of a statistical moment obtained from the RDP reduced model we computed $\mathbb{E}[\mathrm{QOI}_1]$. The error versus number of samples M is reported in Figure 3.4 (right), and its decay is very similar to that of the cross-validated error. We see that in this example RDP is clearly superior to a simple Monte Carlo approximation of the same expected value, where the error decays with the rate $M^{-1/2}$.

3.2. Example 2: The Darcy model in a domain with an inclusion of random shape. The second example we consider is based on problem (3.8), but now we choose a deterministic value of the diffusion coefficient μ as

$$\mu(\mathbf{x}, Y) = \begin{cases} 1, & \Omega_I, \\ 10^{-6}, & \Omega \setminus \Omega_I, \end{cases} \tag{3.13}$$

and the randomness is in the radius of the circular inclusion Ω_I, which is centered in $(0.4, 0.4)$ and has a radius R which is determined by the uniform random variable $Y \sim \mathcal{U}(-1, 1)$ as $R = (Y+2)/10$. For each realization of the random variable we remesh the whole domain. The motivation for this example is to investigate

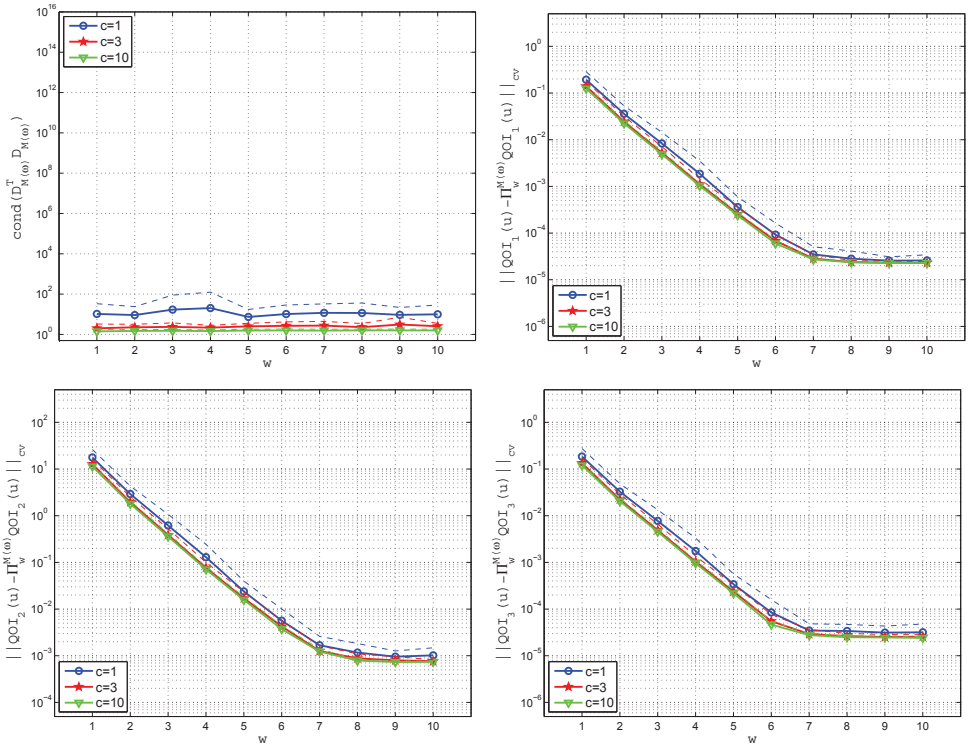

FIG. 3.5. *Example* 2. *Condition number* (3.5) *(top-left) and approximation errors* (3.2) *in the* QOI_i, $i = 1, 2, 3$, *using* $M = c \cdot (\#\Lambda)^2 = c \cdot (\mathrm{w}+1)^2$. *Continuous lines: sample mean averaged over* $R = 100$ *repetitions. Dashed lines: sample mean plus one sample standard deviation averaged over* $R = 100$ *repetitions.*

the effect of a discontinuity of the diffusion coefficient with random location in the physical domain. The discontinuity consists in the boundary of the inclusion where the diffusion coefficient jumps by six orders of magnitude. The QOIs considered are the same as those in Example 1.

Figure 3.5 shows the condition number (3.5) and the approximation error (3.2) in the QOIs in Example 2. In Figure 3.5 we observe an exponential convergence with respect to w up to $\mathrm{w} = 6$ for all three QOIs, and this example shows that these are smooth QOIs even if the problem presents discontinuities with a random location (hence the solution itself, measured in the $L^2(\Omega)$ or $H^1(\Omega)$ norm, is not smooth with respect to $\mathbf{Y}$). For larger values than $\mathrm{w} = 6$ the error levels out due to nonnegligible contributions of the finite element error.

Note again that, as the value of the proportionality constant c increases, the curves converge to the optimal curve corresponding to the exact L^2 projection error curve. In this case, already $M = 3 \cdot (\#\Lambda)^2$ yields the optimal convergence rate.

Example 2*: A less smooth QOI.* We now build a QOI that exhibits a less regular dependence on the random variable $\mathbf{Y}$. We consider again problem (3.8) with the value of the diffusion coefficient μ given by

$$\mu(\mathbf{x}, Y) = \begin{cases} 1, & \Omega_I, \\ 10^{-2}, & \Omega \setminus \Omega_I, \end{cases} \tag{3.14}$$

and the circular inclusion Ω_I with random radius as in the previous section. Note that the discontinuity of the coefficient is a jump of two orders of magnitude across the boundary of the inclusion. Now we consider the following quantities of interest:

$$\text{QOI}_4(Y) = u(\widetilde{\mathbf{x}}, Y)\Big|_{\widetilde{\mathbf{x}}=(0.4,0.4)}, \qquad \text{QOI}_5(Y) = u(\widetilde{\mathbf{x}}, Y)\Big|_{\widetilde{\mathbf{x}}=(0.55,0.55)}, \tag{3.15}$$

which are pointwise evaluations of the solution u of problem (3.8) in two fixed positions $\widetilde{\mathbf{x}} = (0.4, 0.4)$ and $\widetilde{\mathbf{x}} = (0.55, 0.55)$. The former coincides with the center of the random shape inclusion and therefore always lies inside it. The latter point may or may not belong to the inclusion, depending on the outcome of the random variable Y that determines the radius of the inclusion. The corresponding results are displayed in Figure 3.6. The QOI associated with the point $\widetilde{\mathbf{x}} = (0.4, 0.4)$ exhibits a faster convergence than the one associated with $\widetilde{\mathbf{x}} = (0.55, 0.55)$, since the discontinuity in the coefficient affects the regularity of the solution exactly in the point where it is evaluated. In this case, the point $\widetilde{\mathbf{x}} = (0.55, 0.55)$ is such that the probability of falling inside the inclusion is approximately twice the probability of falling outside it. Of course there are also QOIs that are hard to approximate, e.g., the one associated with the point $\widetilde{\mathbf{x}} = (0.6, 0.6)$ that falls inside the inclusion with a probability larger than 98%. In this case the use of *importance sampling* techniques (see, e.g., [17]) should be considered.

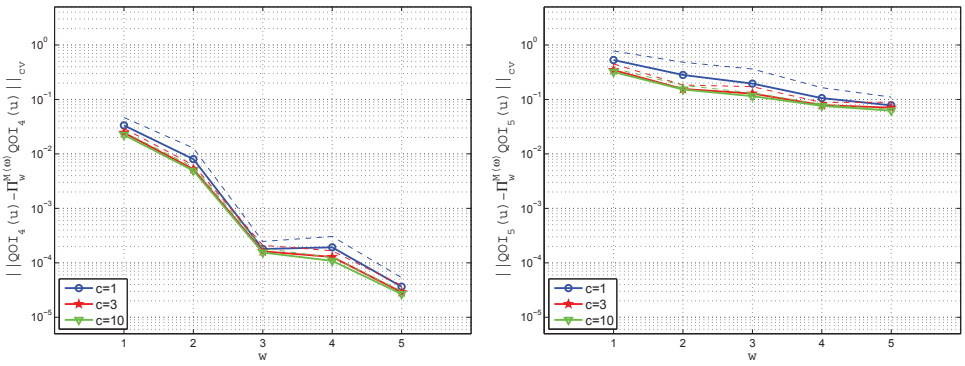

FIG. 3.6. *Example* 2. *Approximation errors* (3.2) *in the* QOI_i, $i = 4, 5$, *using* $M = c \cdot (\#\Lambda)^2 = c \cdot (\mathrm{w}+1)^2$. *Continuous lines: sample mean averaged over* $R = 100$ *repetitions. Dashed lines: sample mean plus one sample standard deviation averaged over* $R = 100$ *repetitions.*

3.3. Example 3: The Darcy flow in a domain with five inclusions. In the next test we again use problem (3.8) and increase the dimension of the parameter space Γ to $N = 5$ by adding some inclusions, as shown in Figure 3.7. The inclusions are circular with radius equal to 0.1 and are centered in the points $\mathbf{x} = (0.5, 0.5)$ and $\mathbf{x} = (0.5 \pm 0.25, 0.5 \pm 0.25)$. We denote by Ω_i, $i = 1, \ldots, 5$, the inclusion domains and by $\Omega_0 = \Omega \setminus \cup_{i=1}^5 \Omega_i$ the bulk. Therefore $\Omega = \bigcup_{i=0}^5 \Omega_i$, and the sets Ω_i are not overlapping each other. The random diffusion coefficient now depends on a multivariate uniform random variable $\mathbf{Y} \sim \mathcal{U}([-1, 1]^5)$ and is defined as

$$\mu(\mathbf{x}, \mathbf{Y}) = \begin{cases} \exp(\beta\, Y_i), & \Omega_i, \quad i = 1, \ldots, 5, \\ 10^{-4}, & \Omega_0 \end{cases} \tag{3.16}$$

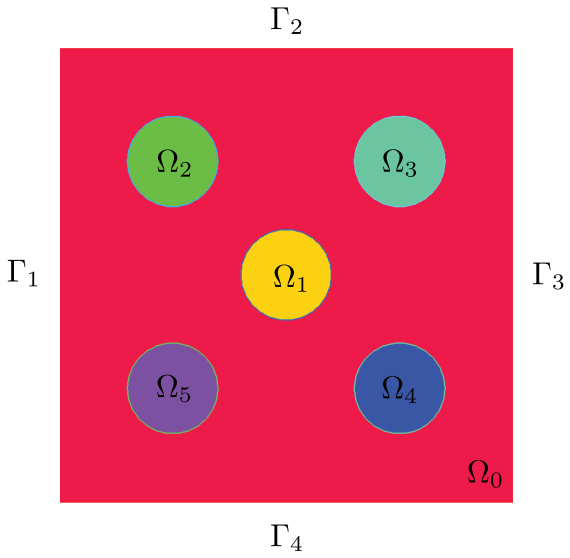

FIG. 3.7. *Domain with five inclusions* $\Omega_1, \Omega_2, \Omega_3, \Omega_4, \Omega_5$ *with random diffusivity for problem* (3.8).

such that each random variable is associated with an inclusion. We consider the same QOIs as in Example 1. The chosen polynomial space $\mathbb{P}_\Lambda$ is the isotropic TD space. As mentioned in the introduction, this choice is motivated by the analysis in [2]. We set $\beta = 2$, so that the coefficient variations in the inclusions are of two orders of magnitude, and report the results in Figure 3.8. The convergence rate is exponential whenever the value of c is larger than 1. A number of points $M = 3 \cdot \#\Lambda$ is enough to achieve the optimal convergence rate, and no deterioration is observed up to the maximal polynomial degree $\mathrm{w} = 10$ considered. Then we set $\beta = 5$ and obtain the results in Figure 3.9. Note that this case yields a variation of more than four orders of magnitude in the coefficient inside the inclusions. As a consequence we observe that the convergence remains exponential but with a slower rate.

3.4. Example 4: The cantilever beam. We consider the *Navier–Lamé* equation written in displacement form on the domain $\Omega = \cup_{i=1}^{7} \Omega_i$ depicted in Figure 3.10:

(3.17)
$$\begin{cases} -(\lambda(\mathbf{x},\mathbf{y}) + \mu(\mathbf{x},\mathbf{y}))\nabla(\nabla \cdot \mathbf{u}) + \mu(\mathbf{x},\mathbf{y})\nabla^2 \mathbf{u} = -f(\mathbf{x},\mathbf{y}), & \mathbf{x} \in \Omega,\ \mathbf{y} \in \Gamma, \\ \sigma(\mathbf{u}) \cdot \mathbf{n} = 0, & \mathbf{x} \text{ on } \partial\Omega \setminus \Gamma_{wall},\ \mathbf{y} \in \Gamma, \\ \mathbf{u} = \mathbf{0}, & \mathbf{x} \text{ on } \Gamma_{wall},\ \mathbf{y} \in \Gamma, \end{cases}$$

with

$$\mu(\mathbf{x},\mathbf{Y}) = \frac{E(\mathbf{x},\mathbf{Y})}{2(1+\nu)}, \qquad \lambda(\mathbf{x},\mathbf{Y}) = \frac{\nu\, E(\mathbf{x},\mathbf{Y})}{(1+\nu)(1-2\,\nu)},$$

and with σ the usual stress tensor

$$\sigma(\mathbf{u}) = \lambda(\nabla \cdot \mathbf{u})\mathbf{I} + 2\,\mu\,\frac{\nabla \mathbf{u} + \nabla^T \mathbf{u}}{2}.$$

Young's modulus E is affected by uncertainty, and it depends on the random variable $\mathbf{Y} \sim \mathcal{U}([-1,1]^7)$ in the following way:

$$E(\mathbf{x},\mathbf{Y}) = \exp(7 + Y_i) \quad \text{in } \Omega_i, \qquad i = 1, \ldots, 7.$$

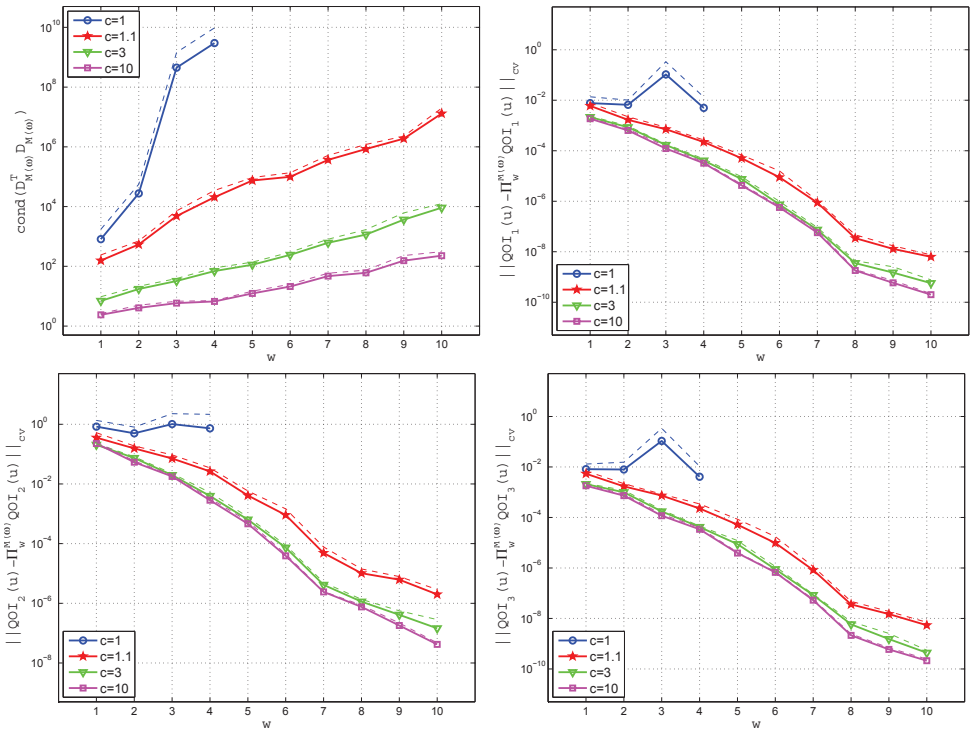

FIG. 3.8. *Example* 3: *the Darcy model.* $\beta = 2$. *Condition number* (3.5) *(top-left) and approximation errors* (3.2) *in the* QOI_i, $i = 1, 2, 3$, *using* $M = c \cdot \#\Lambda = c \cdot (\mathrm{w} + 1)$. *Continuous lines: sample mean averaged over* $R = 100$ *repetitions. Dashed lines: sample mean plus one sample standard deviation averaged over* $R = 100$ *repetitions.*

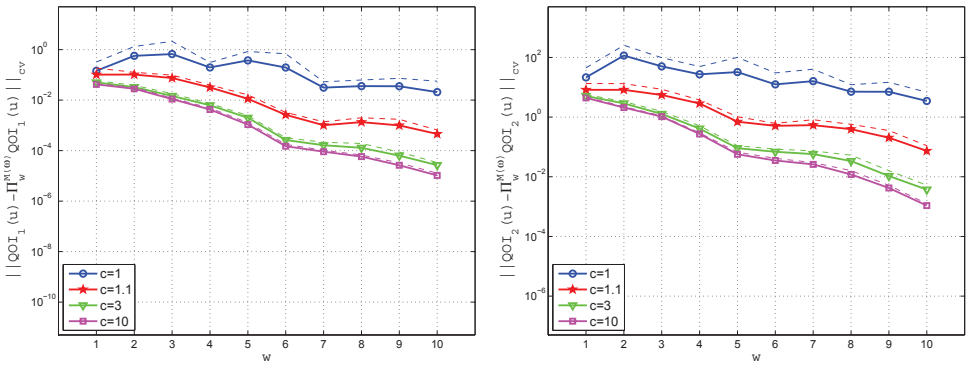

FIG. 3.9. *Example* 3: *the Darcy model.* $\beta = 5$. *Approximation errors* (3.2) *in the* QOI_i, $i = 1, 2$, *using* $M = c \cdot \#\Lambda = c \cdot (\mathrm{w}+1)$. *Continuous lines: sample mean averaged over* $R = 100$ *repetitions. Dashed lines: sample mean plus one sample standard deviation averaged over* $R = 100$ *repetitions.*

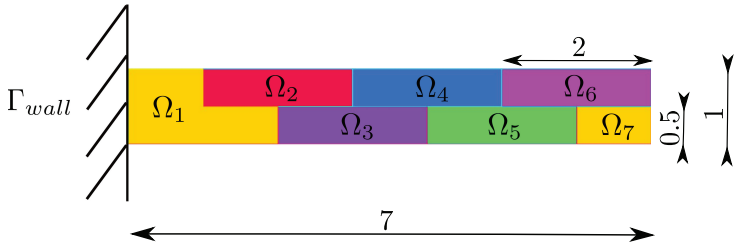

FIG. 3.10. *The cantilever beam.*

Poisson's ratio ν is deterministic and equal to 0.28. The prescribed boundary conditions are null displacement on Γ_{wall} and null stress on $\partial\Omega \setminus \Gamma_{wall}$. The forcing term $f \equiv -1$ models the distributed action of the gravity force. The reference configuration of the cantilever is a 1×7 rectangle. Further details about the geometry are given in Figure 3.10. As in Example 3, we choose $\mathbb{P}_\Lambda$ to be the isotropic TD space. We are interested in the following QOIs:

$$\mathrm{QOI}_6(\mathbf{u}) = \int_\Omega |\nabla u_1|^2 + |\nabla u_2|^2 \, d\Omega,$$

$$\mathrm{QOI}_7(u_2) = \min_{\mathbf{x}\in\Omega} u_2(\mathbf{x}), \qquad \mathrm{QOI}_8(\mathbf{u}) = \int_\Omega \sigma_{12}(\mathbf{u}) \, d\Omega.$$

In Figure 3.11 we report the corresponding results. The convergence is exponential even with $M = 1.1 \cdot \#\Lambda$, which is very close to the minimal number of points required to have an overdetermined problem. The red (star) line corresponds to the choice $M = 3 \cdot \#\Lambda$ and can be considered the optimal convergence rate, since no significant improvement is observed when going to $M = 10 \cdot \#\Lambda$ (green (inverted triangle) line).

3.5. Example 5: Navier–Stokes equations in a random domain. In the last example, we consider the steady state incompressible Navier–Stokes equations which govern the motion of a fluid in a pipe:

$$\begin{cases} -\nu\Delta\mathbf{u} + (\mathbf{u}\cdot\nabla)\mathbf{u} + \nabla p = 0 & \text{in } \Omega, \\ \nabla\cdot\mathbf{u} = 0 & \text{in } \Omega, \\ + \text{ boundary conditions} & \text{on } \partial\Omega. \end{cases} \tag{3.18}$$

The presence of uncertainty in the model is described by a two-dimensional uniform random variable $\mathbf{Y} \sim \mathcal{U}([-1,1]^2)$. The first component Y_1 models the uncertainty in the kinematic viscosity $\nu(\mathbf{Y}) = 10^{-Y_1}$, while the second component determines the geometrical parameter r_1 by

$$r_1 = \frac{1.5 + Y_2}{5}.$$

The parameter r_1 defines the curvature in the innermost part of the elbow of the pipe. The parameter $r_2 = 0.3$ is kept fixed, since it has a minor influence on the solution of the model. The size of the inflow and outflow sections of the pipe and other geometrical details are reported in Figure 3.12. We again choose $\mathbb{P}_\Lambda$ to be the isotropic TD space, although the two random variables have clearly different roles.

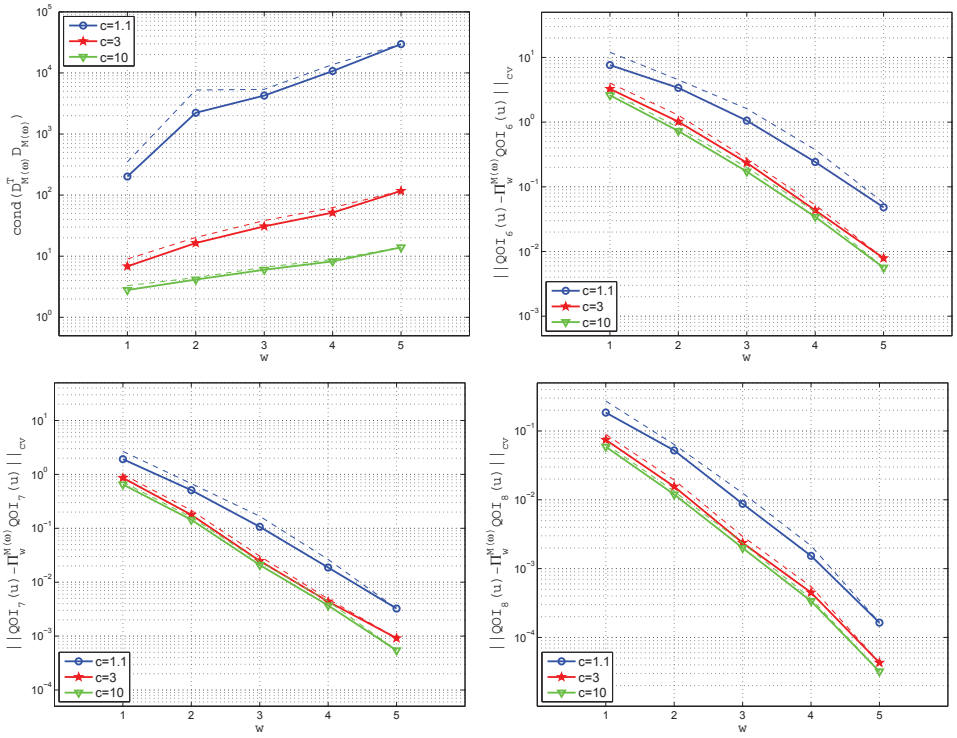

FIG. 3.11. *Example* 4. *Condition number* (3.5) *(top-left) and approximation errors* (3.2) *in the* QOI_i, $i = 6, 7, 8$, *using* $M = c \cdot \#\Lambda = c \cdot (\mathrm{w} + 1)$. *Continuous lines: sample mean averaged over* $R = 100$ *repetitions. Dashed lines: sample mean plus one sample standard deviation averaged over* $R = 100$ *repetitions.*

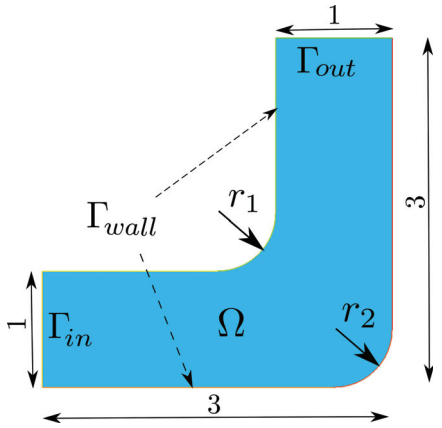

FIG. 3.12. *Geometry of the domain* Ω *in Example* 5.

We impose a Poiseuille velocity profile on Γ_{in} with maximal velocity equal to 4, no-slip conditions on Γ_{wall}, null tangential velocity, and null pressure on Γ_{out}. The QOIs that we address are given by the pressure as

$$\mathrm{QOI}_9(\mathbf{Y}) = \frac{1}{|\Gamma_{\mathrm{in}}|}\int_{\Gamma_{\mathrm{in}}} p(\mathbf{x},\mathbf{Y})\,d\Omega, \qquad \mathrm{QOI}_{10}(\mathbf{Y}) = p(\tilde{\mathbf{x}},\mathbf{Y})\Big|_{\tilde{\mathbf{x}}=(2.5,1)},$$

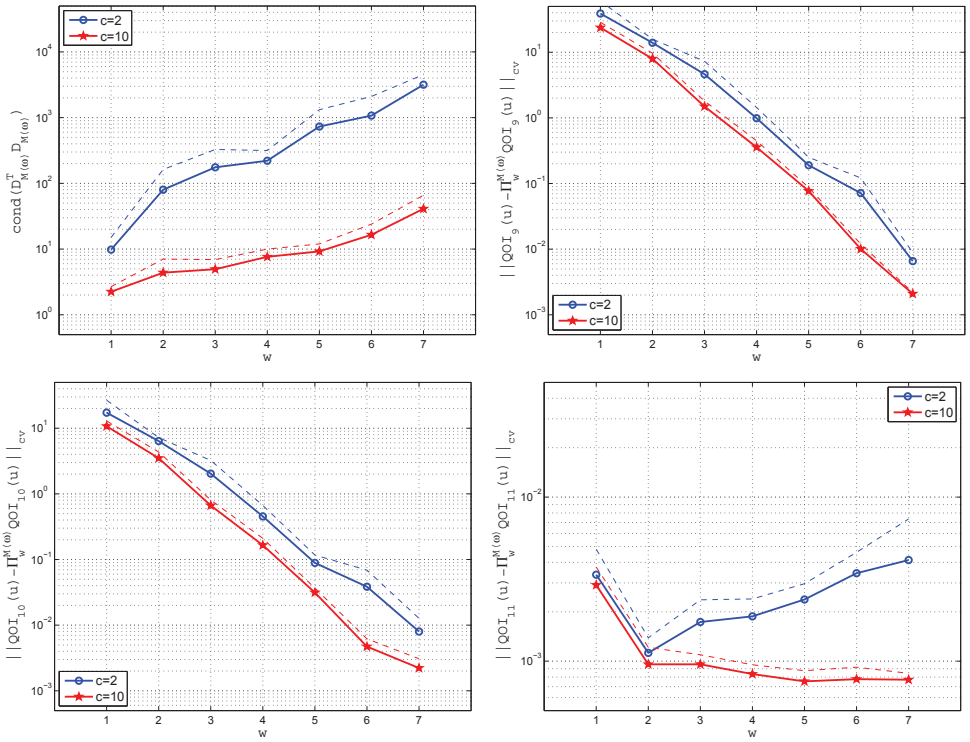

FIG. 3.13. *Example* 5. *Condition number* (3.5) *(top-left) and approximation errors* (3.2) *in the* QOI_i, $i = 9, 10, 11$, *using* $M = c \cdot \#\Lambda = c \cdot (\mathrm{w}+1)$. *Continuous lines: sample mean averaged over* $R = 5$ *repetitions. Dashed lines: sample mean plus one sample standard deviation averaged over* $R = 5$ *repetitions.*

and by the vorticity $\mathbf{v}(\mathbf{x}, \mathbf{Y}) = \nabla \times \mathbf{u}(\mathbf{x}, \mathbf{Y})$ as

$$\mathrm{QOI}_{11}(\mathbf{Y}) = \int_\Omega |\mathbf{v}(\mathbf{x}, \mathbf{Y})| \, d\Omega.$$

The point $\widetilde{\mathbf{x}} = (2.5, 1)$ lies in a central region of the domain where the pressure is largely affected by the values of the random parameters. The Reynolds number ranges from 0.4 to 40, depending on the realizations of the random variable $\mathbf{Y}$. The flow of the fluid is always in the laminar regime.

We report the numerical results obtained in Figure 3.13. The QOIs associated with the pressure converge exponentially fast. On the other hand, the QOI with the vorticity is very sensitive to the input parameters. As a consequence, the corresponding QOI exhibits a slow convergence, and the use of a high order polynomial approximation seems ineffective.

4. Conclusions. In this work we have presented the use of RDP to approximate QOIs related to the solution of PDEs with stochastic data. We have proposed several examples of QOIs related to the solution of the Darcy model, the linear elasticity model, and the Navier–Stokes equations, containing few random parameters, and we have shown numerically how the sample size affects the convergence rate, when using a linear proportionality relation $M \propto \#\Lambda$ or a quadratic relation $M \propto (\#\Lambda)^2$.

For a one-dimensional parameter space, the theoretical analysis proposed in [16] ensures that when a quadratic proportionality $M \propto (\#\Lambda)^2$ is employed, the error com-

mitted by the random projection behaves as the best approximation error in the L^∞ norm. The first two numerical examples proposed, concerning the Darcy model with one random parameter describing either the permeability in an inclusion contained in the domain or the radius of the inclusion, confirm the theoretical results. The QOIs analyzed are all analytic functions of the random parameter, and exponential convergence has been obtained when employing a quadratic proportionality relation $M \propto (\#\Lambda)^2$. On the other hand, with a linear proportionality relation $M \propto \#\Lambda$, the error decays initially exponentially, but a deterioration of the convergence is observed for high polynomial degrees (above $\mathrm{w} = 11$ in Figure 3.4).

The situation seems to be more favorable in higher dimension. Indeed, in all the proposed numerical tests with smooth (analytic) QOIs and more than one parameter, a linear proportionality relation $M \propto \#\Lambda$ yielded an almost-optimal exponential convergence rate, and no deterioration of the convergence due to an insufficient sample size has been observed in the range of polynomial degrees and tolerances tested. The design matrix $(D^\omega)^T D^\omega$ is also better conditioned than in the monovariate case. Although we can not exclude a blow-up of the error for high polynomial degrees, our conclusion is that for practical engineering tolerances, a linear proportionality $M = c \cdot \#\Lambda$ is acceptable, and the higher the dimension, the smaller the constant can be taken, which makes RDP an attractive technique for moderately high dimensional problems. However, a theoretical result supporting this statement is still missing.

The overall efficiency of RDP has to be compared with classical methods such as stochastic Galerkin and stochastic collocation on sparse grids. The RDP is more suited to complex applications than stochastic Galerkin, since the evaluations of the target function are completely uncoupled and one might use a black box deterministic solver. In addition, RDP is very promising for intermediate to large dimensions and could be competitive with or even better than stochastic collocation on sparse grids in terms of accuracy versus number of evaluations of the target function. A fair comparison between the two methods is out of the scope of the present paper and will be addressed in a forthcoming work. Meanwhile, in this paper, we have shown one example of the approximation of the expected value of a QOI, where RDP clearly outperforms a basic Monte Carlo method.

Finally, we remark that a potential great improvement in the stability and consequent efficiency of RDP could be achieved by sampling from a distribution different from the underlying one, as mentioned in Remark 2. This aspect will be investigated in a future work.

REFERENCES

[1] I. Babuška, F. Nobile, and R. Tempone, *A stochastic collocation method for elliptic partial differential equations with random input data*, SIAM Rev., 52 (2010), pp. 317–355.

[2] J. Beck, F. Nobile, L. Tamellini, and R. Tempone, *Convergence of quasi-optimal stochastic Galerkin methods for a class of PDEs with random coefficients*, Comput. Math. Appl., to appear.

[3] B. Blatman and B. Sudret, *Sparse polynomial chaos expansions and adaptive stochastic finite elements using regression approach*, C. R. Mécanique, 336 (2008), pp. 518–523.

[4] H. J. Bungartz and M. Griebel, *Sparse grids*, Acta Numer., 13 (2004), pp. 147–269.

[5] A. Cohen, M. A. Davenport, and D. Leviatan, *On the stability and accuracy of least squares approximations*, Found. Comput. Math., to appear.

[6] A. Cohen, R. Devore, and C. Schwab, *Analytic regularity and polynomial approximation of parametric and stochastic elliptic PDE's*, Anal. Appl. (Singap.), 9 (2011), pp. 11–47.

[7] M. Eldred, *Design under uncertainty employing stochastic expansion methods*, Int. J. Uncertain. Quantif., 1 (2011), pp. 119–146.

[8] M. Eldred, C. Webster, and P. Constantine, *Evaluation of non-intrusive approaches for Wiener-Askey generalized polynomial chaos*, in Proceedings of the 10th AIAA Non-Deterministic Approaches Conference, Schaumberg, IL, 2008, American Institute of Aeronautics and Astronautics, Reston, VA, 2008, AIAA-2008-1892.

[9] O. G. Ernst, A. Mugler, H.-J. Starkloff, and E. Ullmann, *On the convergence of generalized polynomial chaos expansions*, ESAIM Math. Model. Numer. Anal., 46 (2012), pp. 317–339.

[10] B. Ganapathysubramanian and N. Zabaras, *Sparse grid collocation schemes for stochastic natural convection problems*, J. Comput. Phys., 225 (2007), pp. 652–685.

[11] R. Ghanem and P. D. Spanos, *Stochastic Finite Elements: A Spectral Approach*, Dover, New York, 2003.

[12] L. Györfi, M. Kohler, A. Krzyżak, and H. Walk, *A Distribution-free Theory of Nonparametric Regression*, Springer-Verlag, New York, 2002.

[13] S. Hosder, R. W. Walters, and M. Balch, *Point-collocation non-intrusive polynomial chaos method for stochastic computational fluid dynamics*, AIAA J., 48 (2010), pp. 2721–2730.

[14] O. P. Le Maitre and O. M. Knio, *Spectral Methods for Uncertainty Quantification*, Springer, New York, 2010.

[15] G. Migliorati, *Polynomial Approximation by Means of the Random Discrete L^2 Projection and Application to Inverse Problems for PDEs with Stochastic Data*, Ph.D. thesis, Dipartimento di Matematica "Francesco Brioschi," Politecnico di Milano, Milano, Italy, and Centre de Mathématiques Appliquées, École Polytechnique, Palaiseau, France, 2013.

[16] G. Migliorati, F. Nobile, E. von Schwerin, and R. Tempone, *Analysis of the Discrete L^2 Projection on Polynomial Spaces with Random Evaluations*, MOX report 46-2011, Politecnico di Milano, Milano, Italy, submitted.

[17] C. P. Robert and G. Casella, *Monte Carlo Statistical Methods*, Springer-Verlag, New York, 2004.

[18] D. Xiu and G. E. Karniadakis, *The Wiener–Askey polynomial chaos for stochastic differential equations*, SIAM J. Sci. Comput., 24 (2002), pp. 619–644.